Enhanced Catalytic Activity in the Oxidative Synthesis of Benzoxazoles by Tuning Local Electron Charge Densities in N-doped sp3@sp2 Hybrid Nanodiamond

Qingqing Gu
Dalian Institute of Chemical Physics
Yanan Zhou
Sichuan University
Rui Huang
Dalian University of Technology https://orcid.org/0000-0002-3276-6137
Yangming Lin
MPI for Chemical Energy Conversion
Chi Xu
Dalian Institute of Chemical Physics
Qian Jiang
Dalian Institute of Chemical Physics, Chinese Academy of Sciences
Siglinda Perathoner
University of Messina https://orcid.org/0000-0001-8814-1972
Gabriele Centi
Univ. of Messina, INSTM and ERIC aisbl https://orcid.org/0000-0001-5626-9840
Yuefeng Liu (yuefeng.liu@dicp.ac.cn)
Dalian Institute of Chemical Physics https://orcid.org/0000-0001-9823-3811

Article

Keywords: Carbocatalysis, N-doped sp3@sp2 hybrids nanocarbon, surface electronic structure tuning, aerobic liquid-phase reaction, drugs synthesis

Posted Date: May 17th, 2021

DOI: https://doi.org/10.21203/rs.3.rs-515078/v1

Abstract

Metal-free nanocarbons among other unique characteristics, offer the possibility of tuning the local electronic structure of the active sites allowing to identify precisely how to enhance the catalytic activity. Hence N-doped sp^3@sp^2 hybrid nanocarbons are studied here for the catalytic oxidative synthesis of a broad series of drug-related compounds (23 examples), like 2-substituted benzoxazoles, benzothiazoles and benzimidazoles under mild conditions and they show good catalytic activity and reusability which is comparable to homogeneous /heterogeneous metal-based catalysts. We demonstrate for the first time that the electron-donating capability and intrinsic catalytic activity of pyridinic N and neighboring C atoms can be enhanced by increasing up to c.a. 3 layers of sp^2 C over the N-doped sp^3@sp^2 nanocarbon, which is evidenced by the KPFM measurements and DFT calculations. The mechanistic study suggests that the O_2 could be activated to $O_2^{\bullet-}$, which could subsequently react with abstracted H along with the formation of H_2O_2. This study provides a methodology of applying carbocatalysts for the synthesis of complex drug targets and shed light on the origin of the intrinsic catalytic activity enhancement of the pyridinic N by regulating the sp^2 C layers of the catalysts.

Introduction

Five-membered heterocyclic rings, such as benzoxazoles, benzothiazoles and benzimidazoles, are important building blocks for natural products, bioactive molecules, pharmaceutical and agrochemical compounds[1, 2]. One of the typical methods for preparation of five-membered heterocyclic framework involves the condensation of 2-amino phenol/thiophenols/anilines and carboxylic acids, aldehydes or alcohols to form 2-(benzylideneamino)phenol (intermediate, **I**) and followed by annulation and oxidative dehydrogenation using strong oxidants (DDQ[3], $Th^+ClO_4^-$[4],ozone[5], etc). To avoid these stoichiometric oxidants in the catalytic process and to improve atom economic process, using a cheap oxidant such as O_2, is a relevant target for achieving green chemistry. Recently, synthesizing the five-membered heterocyclic framework in the presence of O_2 molecules has received much attention. For example, aminoxyl radicals (e.g, 4-methoxy-TEMPO[1]), metal complexes (Ru–xantphos[2], CuI/TEMPO/Bpy[6], $Zn(OAc)_2$[7], etc) and metal nanoparticles (Au/TiO_2[8], Pt nanocluster[9], $AgPd/WO_{2.72}$[10], etc) have been proved to be efficient catalysts for the aerobic catalytic synthesis of benzoxazole framework. Their catalytic activities originate from the agostic interaction endowed by their strong electron-acceptor/donor properties, which could efficiently facilitate the hydrogen abstraction from the O-H bond of the phenol moiety of **I,** which is a key reaction step for the synthesis of benzoxazoles. Regardless of the progress made in metal-based catalysts, many issues are still present in catalyst recovery and recycle, costs and stability, and especially metal leaching during the reaction. In addition, for the use of these products in many pharmaceutical applications, the presence of residual metals even in ppb levels must be avoided. Hence, it is desirable to develop the efficient and environmentally friendly synthetic strategies for metal-free heterogeneous aerobic catalytic synthesis of heterocycles. Metal-free nanocarbons offer from this

perspective unique characteristics, and they have been demonstrated in various catalytic reactions.[11, 12, 13, 14, 15, 16]

Benefited from the superior thermal and chemical stability, high curvature, unique electronic structure and good electron-acceptor/donor properties, sp^3@ sp^2 hybrid nanocarbons (nanodiamond-derived) have been proved to be efficient catalysts for various catalytic transformations.[17, 18, 19, 20, 21] Nitrogen (N) doping is an efficient strategy to improve the catalytic activity of nanocarbons since it could induce charge transfer and redistribution between doping sites and neighboring carbon and thus enhance the O_2 adsorption in ORR[22], facilitate the activation of α-H of -CH_2OH in catalytic oxidation of different alcohols[23], etc. The combination of N doping and sp^3@sp^2 hybrid nanocarbons can create unique materials with peculiar catalytic reactivity.[24]

By analogy to single atom catalysts, the catalytic activity of isolated active N species on the surface of nanocarbon could be largely influenced by the coordination environments and host property.[25, 26] Large efforts have applied to identify the catalytic activity of different N species (N in different coordination environment) to understand the detailed catalytic mechanism and increase the density of active sites to improve the catalytic activity [22, 27, 28, 29]. However, enhancing the intrinsic catalytic activity of specified N groups by tuning the electron property of the host and exploiting the synergy between N doping and sp^3@sp^2 hybrid nanocarbon structure remain challenging. In terms of fundamental understanding, the study of these aspects offers the unique possibility to obtain precise correlations between surface charge density of the N species and nearlying carbon atoms and catalytic activity. This offers unmatched prospects to advance in mechanistic understanding, and to develop novel catalytic options.

To address these aspects, we report herein the first general strategy for aerobic synthesis of benzoxazoles with o-aminophenol and benzaldehyde catalyzed by N-doped sp^3@ sp^2 hybrid nanocarbon (Scheme 1). These nanodiamond-like materials are characterized by a few layer, N-doped sp^2 layer (graphene-like) surrounding a sp^3-core.[12,23] The catalytic system is characterized by mild condition of operations, wide substrate scope, high selectivity and yields. The catalytic performance and surface properties of N-doped sp^3@ sp^2 hybrid could be enhanced by tuning N species and the sp^2 carbon contents. By combining different physico-chemical methods including Raman, X-ray photoelectron spectroscopy (XPS) and electron energy loss spectroscopy (EELS), we demonstrate here that pyridinic N sites are the active sites for the oxidative synthesis of benzoxazoles. However, there is also a contribution of sp^2 carbon layers in promoting the intrinsic catalytic activity of these pyridinic N sites. By the control experiments, work function analysis and density functional theory (DFT) calculations, we revealed that the higher sp^2 carbon layers could endow the surface active sites higher electron density and enhance the interfacial charge transfer with the adsorbed intermediates I and O_2, thus catalyzing more effectively the process.

Results

The catalytic performance of N-doped sp^3@ sp^2 hybrid nanocarbon

N-doped sp^3@sp^2 hybrid nanocarbon was prepared starting from nanodiamond (ND) which is annealed at 900°C with a nitrogen precursor. The scheme of preparation of this NC@ND-900 catalyst is presented in Fig. S1 and is characterized by a single layer discontinuous curved sp^2 carbon layer on the surface (Fig. 1a). The N content is 3.7 at% (Fig. 1b) with four configurations including pyridinic N (N1, 398.5 eV), pyrrolic N (N2, 400.1 eV), graphitic N (N3, 401.1 eV) and N oxide (N4, 403.2 eV) [22]. The homogeneous distribution of N species was further confirmed by energy-dispersive X-ray spectroscopy (EDS) mapping (Fig. S2) results.

The aerobic synthesis of 2-phenylbenzoxazole (**P**, target product) by o-aminophenol (**A**) and benzaldehyde (**B**) was chosen as model reaction (see top of Fig. 1) to explore the catalytic performance of ND-based nanocarbons catalysts. Without the catalyst (Fig. 1c), 96.1% of **A** could be exclusively converted into **I** (2-(benzylideneamino phenol, intermediate) with 99.8% of selectivity but the product **P** was undetected. The condensation reaction between the amino-group (**A)** and aldehyde-group (**B**) is occurring easily without catalyst, while the following dehydrogenation and annulation steps between the -OH group and imide C-H bond of **I** requires a catalyst. The pristine NDs (i.e. before N introduction) used as catalyst gives only traces of P (Fig. 1c). After the oxygen and nitrogen groups were introduced by HNO_3/H_2SO_4 treatment (oND900) and followed by NH_3 post-treatment (NoND900), respectively, the catalytic performance was not affected significantly. NC@ND-900 catalyst instead shows a remarkably enhanced formation of **P (**9.6%, structure confirmed by GC-MS in Fig. S3**)** compared to the NoND900, indicating the important role of N doping, but also the relevance of the methodology of its introduction. Note that substituting O_2 in the reaction atmosphere with N_2, no product **P** was detected, indicating that O_2 is indispensable to the dehydrogenation step of **I** (Fig. 1c). To optimize the performances and understand better the catalytic behavior, the role of reaction temperature and time were further investigated (Fig. 1c and Table S1).The selectivity of **P** increases with reaction time and reaching the value of 97.4% at 28 h, which is comparable with the homogeneous or heterogeneous metal-based catalytic systems (Table S2). Notably, the stability of NC@ND-900 was investigated and it could be applied to 5 successive cycles with negligible loss of the catalytic efficiency (1^{st} Yield **P** of 79.0% *vs.* 5^{th} Yield **P** of 77.1%, Fig. S4). Given that similar catalytic performance of further purified NC@ND-900-HCl and extra Fe loaded Fe/NC@ND-900 samples to NC@ND-900 (Table S3), the possible contribution of residual metal impurities can be excluded (confirmed by ICP results in Table S4). This indicates that the intrinsic catalytic activity originates from the nanocarbon rather than the residual metal species.

To check the role of the different N species in the NC@ND-900 (see Fig. 1b), their amount was changed by varying the annealing temperature (Fig. S1). Four N-doped sp^3@ sp^2 hybrid nanocarbons were prepared and present decrease tendency of nitrogen contents (from 4.0 at. % for NC@ND-700 to 2.1 at. % for NC@ND-1300) and increase tendency of the sp^2 carbon percentage through increasing the annealing temperature from 700 ^oC to 1300 ^oC (Figs 1d, S5 and Tables S5-S6). The yield of **P** increases from 21.5% to 27.7% as the synthesis temperatures raise from 700 °C to 900 °C and then decreased to 19.1% and

13.1 % as the temperatures increase to 1100 °C and 1300 °C, respectively (Fig. 1e), indicating the significant influence of the annealing temperature on the catalytic activity. The analysis of the relationship among different N species content, sp^2 carbon percentage (derived from XPS results, Fig 1b and Table S5) and catalytic activity shows that a linear relationship is presented only between pyridinic N and sp^2 carbon content normalized catalytic activity (Fig. S6) in the N-doped sp^3@ sp^2 hybrid nanocarbon series (Fig. 1g). This indicates a critical role of pyridinic N in the catalytic activity, but in relation to the sp^2 carbon content of the catalyst.

Influence of sp^2 carbon on the local structure of N species

To study the influence of sp^2 carbon content on the local structure of N species, N-doped sp^3@ sp^2 hybrid nanocarbons with different sp^2 carbon layers was synthesized by using different temperature annealed NDs (NDT, T=900 °C, 1300 °C and 1600 °C) as starting materials rather than the NDs (Fig. 2a and Fig. S1). Then, these samples were doped with N by using the same procedure for NC@ND-900. The obtained samples were referred as NC@ND-C1, NC@ND-C3 and NC@C9 when ND900, ND1300 and ND1600 were applied as starting material, respectively. Compared with the ND particles, which show typical (111) planes of diamond (Fig. 2b), one layer and 3-4 layers of curved sp^2 graphitic-like shell was observed on the surface when ND900 and ND1300 was applied as precursors (Fig. 2c-2d), respectively. While the sp^3 carbon have totally transformed into onion-like carbon when ND1600 was applied as precursor (Fig. 2e). The structure evolution of catalysts was also studied by the UV-Raman, as shown in Fig. 2f and Table S7, the spectrum of NDs exhibits a peak at 1622 cm^{-1} (overlap of G band at 1590 cm^{-1} and -OH bending vibrations at 1640 cm^{-1}) and diamond sp^3 mode at 1324 cm^{-1} [30]. After annealing at high temperature and introduction of N, the diamond peak (1324 cm^{-1}) disappear while the D-mode peak centered at 1400 cm^{-1} appears. This peak originates from the breathing of hexagonal carbon rings with defects.[30] Meanwhile, the G-mode peaks are observed and shifted from 1622 cm^{-1} to 1587 cm^{-1}, indicating the transformation of sp^3-hybridized C into sp^2-hybridized C and the graphitization of sp^2 carbon.[30] The EELS results (Fig. 2g) also confirm this transformation since the intensity of π* peak (285 eV, for sp^2-hybridized carbon) increased with the increasing annealing temperature and also increased slightly after the N-doping process.[31] C1s spectra of XPS results (Fig 2h, Fig.S5 and Table S6) also present the same trend that the sp^2/sp^3 values of the samples increasing from 0.2 of NDs to 2.3 of ND1600. When the N species were introduced, the sp^2/sp^3 values increase from 0.5 of NC@ND-900 to 2.9 of NC@C9. These results clarify the evolution process of sp^3 hybridization C transformed into sp^2 hybridization C (detailed illustration in Fig. S7) and confirm N-doped sp^3@ sp^2 hybrid nanocarbons with different sp^2 carbon layers were successfully synthesized.

The catalytic performance of above samples were investigated in the aerobic synthesis of 2-phenylbenzoxazole. As shown in Fig. 3a, around 7% yields of **P** was observed when the NDs was annealed under 900 °C, 1300 °C and 1600 °C (dark violet bars), suggesting the formed sp^2 carbon layers in the N-free catalysts could contribute trace catalytic activity. For the N-doped samples (dark green bars),

the yield of **P** increased from 27.7 % of NC@ND-900 to 39.2%, 42.0 % and 42.9 % of NC@ND-C1, NC@ND-C3 and NC@C9, respectively, indicating the active site role of N species (pyridinic N). By normalizing the reaction rate of **P** (λ_P) by the pyridinic N content (Fig. 3a), a clear enhancement of the value is observed on increasing the sp^2 carbon layer up to about 3, while not further increasing when the sp^2 carbon layers increase from 3 layers to ca. 9 layers (NC@C9). The results confirmed the contribution of sp^2 carbon layers to the intrinsic catalytic activity of pyridinic N. To understand the role of inner sp^3 C core, an equivalent sample to NC@ND-900 was prepared, but having as inner core SiO_2 sphere (ca. 20 nm) (NC@SiO_2). This sample shows 9.4% yield of **P** and when λ_P is normalized to pyridinic N, the value is very similar to that of NC@ND-900. This indicated that the sp^3 C core has only the function of stabilizing and forming the surface sp^2 C layer, although favouring forming more pyridinic N sites.

To address the role of the sp^2 carbon layers in the enhancement of the catalytic activity, local work functions obtained from Kelvin probe force microscope (KPFM) measurements was used to evaluate the electron donating capability of N-doped samples (Fig 3b)[32]. Theoretically, the electron-donating capability of catalysts determines the interfacial charge transfer to the associated reactants, with a profound significance.[27, 33] Fig. S8 shows the topographical and CPD (contact potential difference) images simultaneously taken on different samples. As shown in the Fig 3b, NC@ND-900 presents the highest work function (4.99 eV). When the sp^2 carbon layers were increased, the work function of NC@ND-C1 and NC@ND-C3 decreased to 4.92 eV and 4.79 eV, respectively, which indicates their higher electron-donating capability. The NC@C9 presents similar work function compared to NC@ND-C3 even through NC@C9 contain more sp^2 carbon layers, indicating that the further increases in the number of sp^2 C layers do not influence further the work function and the interfacial charge transfer. Thus, the intrinsic catalytic activity of pyridinic N could be further improved by increasing sp^2 carbon layer (up to about three) and the associated influence on the work function induces a change in the electron-donating capability.

To proof this conclusion, DFT calculations were made to investigate the enhanced catalytic activity on increasing sp^2 carbon layers up to three (see Methods section for more details of calculation). Being the activation of O_2 a key reaction step of the aerobic synthesis of **P**, attention was focused on the interaction between O_2 and different model catalyst structures: a pyridine-N doped graphene coated on NDs (**structure A**), 2 layers graphene covered NDs (**structure B**) and 4 layers graphene (**structure C**) (Fig S9). Fig.3c and Fig S10 show the most stable optimized configurations of O_2 molecule adsorbed on three model structures. We can clearly see that the most stable adsorption site for O_2 is the more positively charged C atom that adjacent to the pyridinic N atom. The O_2 adsorbed on **structure B** is more stable (-3.52 eV) than that of **structure A** (-2.75 eV), while similar with that of O_2 adsorbed on **structure C** (-3.40 eV). The results indicate that, compared to the pure NDs, the activation of O_2 undergoes an increase trend and then remains similar as increasing the sp^2 carbon layers gradually.

To further understand the interaction between the catalysts and O_2, the charge transfer of different systems were calculated by using Bader charge analysis (Fig S11). In all the analyzed systems, the

electrons are transferred to the adsorbed O_2, the charge transfer (Q) increasing from 0.78 of **structure A** to 0.89 of **structure B** , while slightly decreasing to 0.84 when further increasing the sp^2 C layers (Fig.3c). Compared with **structure A**, the adjacent C atoms of pyridinic N in **structure B** and **structure C** both present more abundant electrons transferred from inner multilayers of graphene, which could promote electron transfer from the catalyst surface to O_2 (Table S8). Additionally, from the calculated partial density of states (PDOS) in Fig. 3d, a stronger hybridization of the p orbital of the C atom that bind with the O_2 and p orbital of the adsorbed O_2 around the Fermi level in **structure B** and **structure C** with respect to **structure A**. This evidence further supports the mechanistic explanation of the interaction between O_2 and catalyst models.

Mechanistic Study

The spin-trapping electron paramagnetic resonance (EPR) technique using 5,5-dimethyl-1-pyrroline N-oxide (DMPO) as the spin trap was performed to obtain information on the activation process of O_2[34]. As shown in Fig. 4a, the catalytic systems with mixture of substrate and catalyst or mixture of substrate and O_2 remain EPR silent after adding DMPO. When substrate, catalyst and O_2 were all presented, the EPR signal of the catalytic system shows the characteristic fingerprint of spin adducts DMPO–•OOH compared with the simulated DMPO–•OOH EPR signal, which resulting from trapping superoxide ($O_2^{\bullet-}$) with DMPO.[35] The results indicate the O_2 activation by N-doped sp^3@ sp^2 nanocarbonsand the generation of reactive $O_2^{\bullet-}$ species, which could be responsible for the oxidative dehydrogenation steps during the synthesis of **P**. It is reasonable to speculate that the H_2O_2 would be formed as intermediate in the $O_2^{\bullet-}$ involved aerobic oxidation reactions. To proof this hypothesis, detection of H_2O_2 was made by using the catalyzed oxidation of N, N-diethyl-1, 4-phenylenediammonium sulphate (DPD) by Horseradish peroxidase (POD).[36] The absorption peaks at around 510 and 551 nm confirm the formation of H_2O_2 during the reaction process (Fig. 4b). The EPR and UV-Vis results indicate that the N-doped sp^3@ sp^2 nanocarbon catalyzed aerobic synthesis of **P** was proceed via superoxide radical ($O_2^{\bullet-}$) involved routine and H_2O_2 was formed as intermediate by hydrogen abstraction from the organic substrate directly or (in)directly. The activation process of **I** was also studied by ATR-IR (Fig. 4c and Fig. S12) and the red shift (from 3329 cm^{-1} to 3324 cm^{-1}) of -OH group of **I** was observed in the presence of model catalyst. The results indicate **I** was activated by the catalysts and the -OH bond was weakened before the H abstraction step.

Based on the results above, a plausible reaction mechanism of intermolecular annulation reaction between 2-phenylbenzoxazole and benzylaldehyde could be proposed. As shown in Fig 4d, initially, the intermediate **I** forms by the condensation of o-aminophenol and benzylaldehyde. Then the formed **I** absorbs on the surface of catalyst and the reaction was initiated with a hydrogen abstraction step of the O-H bond from **I** by catalyst. Then the **I*** undergoes intramolecular cycloaddition of the imine to form the corresponding aminyl radical (**P***). The reaction was followed by the second H abstraction from the **P*** due to the driving force for aromatization and ultimately generate the desired product (**P**). Meanwhile,

after the O_2 was absorbed on the surface of the catalyst, the electron transfer happened from the C atom that adjacent to the pyridinic N to the O_2 to form $O_2^{\bullet -}$, which subsequently react with the protons abstracted by the catalyst to form H_2O_2 and regenerate the active sites.

Substrate scope experiments

Having successfully achieved the aerobic oxidative synthesis of 2-phenylbenzoxazole, it is valuable to analyze how the catalytic system could be applied to the synthesis of other substituted benzoxazoles, benzothiazoles and benzimidazoles by using different substituted 2-aminophenol, 2-aminothiophenol or 2-phenylenediamine respectively with aldehydes as starting materials (Table 1). The reactions with benzaldehydes bearing electron-deficient (**P2** and **P3**) and electron-rich groups (**P4**-**P6**) at the aromatic ring proceeds smoothly to give the desired products in good yields. When the cinnamaldehyde (**P7**) and 4-formyl-trans-stilbene (**P8**) were chosen as reactants, the desired products were produced with yields of 92.6% and 84.4%, respectively. 82.9% yield of **P9** was achieved when the furfural was chosen to provide the aldehyde group. The aliphatic aldehydes were also successfully employed as substrates to give the corresponding products but with relatively lower yields (**P10**-**P11**). After the aldehydes screening, the scope of various 2-aminophenols was also investigated. Functional groups including chloro, nitro, and cyano were well tolerated under the optimal reaction conditions, and the desired products were obtained in moderate to good yields (**P12**-**P14**). The results above indicate that the reactions are insensitive to the electron-donating or election-withdrawing nature of the substitutes. A high yield of 73.3% was obtained when the benzene ring was replaced by a naphthyl group (**P15**). To further validate the general use of the proposed catalytic method, the 2-aminophenols was replaced with 2-aminothiophenol and 2-phenylenediamine for the synthesis of benzothiazoles and benzimidazoles. To our delight, the reactions of 2-aminothiophenol and 2-phenylenediamine with benzaldehyde, furfural and benzaldehydes bearing chloro, nitro and methoxyl groups proceed with good yield as shown in Table 1, **P16**-**P23**.

N-doped sp^3@ sp^2 hybrid nanocarbons are highly effective, stable and valuable metal-free carbocatalysts for the aerobic catalytic oxidative synthesis of various heterocycles including 2-substituted benzoxazoles, benzothiazoles, and benzimidazoles. They can be synthetized with high yields by one pot reaction of aldehydes with 2-aminophenole, 2-amonothiophenol and o-phenylenediamine, respectively. The correlation between catalysts characteristics and performances indicate that pyridinic N and neighboring C atoms are the active sites. The electron-donating capability of pyridinic N surface atoms, and the charge density of neighboring C atom can be modulated by increasing up to three sp^2 C layers of N-doped sp^3@ sp^2 hybrid. Therefore, increasing the sp^2/sp^3 carbon ratio of the N-doped sp^3@ sp^2 hybrid nanocarbon could lead to a higher intrinsic catalytic activity. The mechanistic study well supports this indication and provides evidence that the carbon adjacent to pyridinic N species (with enhanced electron-donating capability) could activate O_2 molecules to yield an oxygen anion radical that react with the abstracted proton on the surface of catalyst, then forming H_2O_2 and regenerating the catalyst simultaneously. It is the first time that it was demonstrated the possibility to enhance the intrinsic catalytic activity of pyridinic N by regulating the sp^2 carbon layers of the catalysts. This study also

demonstrates that the N-doped sp^3@ sp^2 hybrid catalytic system provides an attractive and useful methodology to achieve a green chemistry approach for the one-pot synthesis of important pharmaceutically related products.

Methods

The synthesis of N-doped sp^3@ sp^2 hybrid nanocarbon. The NDs were purchased from the Beijing Grish Hitech Co. and purified by concentrated HCl (37%) solution under room temperature for 6 times (12 h per time) to remove metal impurities from NDs. After washed thoroughly with DI water until neutral pH, the samples were dried in vacuum oven at 60 °C.

To prepare sp^3@sp^2 hybrid nanocarbon with sp^2 carbon layers (denoted as ND-T1, T1=900, 1300 and 1600), the NDs were annealed under 900 °C, 1300 °C and 1600 °C, respectively in Ar atmosphere for 4 h. In a typical preparation of N-doped sp^3@ sp^2 hybrid nanocarbon, 1.5 g of citric acid (99.5%, Sinopharm) and 1.5 g $(NH_4)_2CO_3$ (Analytical Grade, Sinopharm) were dissolved in 5 mL distilled water, followed by an addition of 1.0 g of purified ND and ultrasonication was applied for 30 min to achieve uniform dispersion. Then the obtained mixture was cured in an oven at 130°C for 5 h, followed by a thermal treatment at 700 °C, 900 °C, 1100 °C and 1300 °C under Ar atmosphere for 2 h (3 °C /min), respectively. The obtained samples were named as NC@ND-T2 (T2 refers to the annealing temperature).

To study the influence of the numbers of sp^2 carbon layers, the same preparation process was used with a fixed annealing temperature (900 °C) except the starting material NDs were replaced by ND900, ND1300 and ND1600. The as-prepared samples were denoted as NC@ND-Cx (x refers to the average sp^2 carbon layers, which was statistic numbers obtained from HR-TEM, like NC@ND-C1, NC@ND-C3 and NC@C9). Furthermore, SiO_2 sphere (diameter around 20 nm) as inert insulator was also chosen as starting material using the above method to obtain NC@ SiO_2 (annealing temperature 900 °C).

Typical procedure for the aerobic synthesis of 2-substituted benzoxazoles, benzothiazoles and benzimidazoles. The reactions were performed in a pressure tube. Aminophenol (2 mmol), benzaldehyde (2.2 mmol), 120 mg catalysts and 10 ml of xylene as solvent were added into the 75 mL glass pressure tube followed by exchange with O_2. Then the tube was sealed and maintained at 140 °C for a certain time. After the reaction was finished, the tube was cooled to room temperature and 10 ml EtOH and 200 µL nitrobenzene were added for quantitative analysis with GC (Agilent 7820 with HP-5 column). For the recycling test, the used catalysts were collected by filtration and then washed by EtOH. Then the new reactants and solvent were added for the next run.

Detecting superoxide radical anion. Typical spectrometer parameters: microwave power 20 mW, microwave frequency 9.4 GHz, scan time 60 s, modulation amplitude 0.02 mT, modulation frequency 100 kHz. For the EPR test, 5, 5-dimethyl-1-pyrroline N-oxide (DMPO) was used as radical trapper and dissolved in EtOH to prepare 20 mg/mL DMPO solution. The different reactions were performed like describe above,

after 2 h reaction, the reaction solution was quickly taken out into a small tube followed by adding DMPO solution. Then the mixture was measured by EPR.

Detecting H_2O_2. The evolved H_2O_2 in the catalytic process was measured by using the colorimetric DPD method. The DPD method is based on the oxidation of N, N-diethyl-phenylenediamine (DPD) catalyzed with horseradish peroxides (POD) by H_2O_2. Briefly, 0.1 g of DPD was dissolved in 10 mL H_2O, denoted as solution A. 0.1 mg peroxidase (POD) was dissolved in 10 mL water, denoted as solution B. After reaction 10 mL H_2O was added into the reaction solution and the mixture was further stirred thoroughly to extract the H_2O_2 from the organic phase to the water. After the stirring, the H_2O_2 containing water was separated from the organic solvent and then 0.5 mL water was token and further diluted with 4 mL DI water, denote as solution C. Finally, 4.5 mL solution C, 0.5 mL phosphorous buffer solution (pH 6.7), 10 µL solution A and 10 µL solution B were mixed for the e ultraviolet-visible spectra test.

KPFM measurements. For the CPD (contact potential difference) measurements, samples were prepared by transferring the samples onto a single crystal Cu (111) substrate using a drop-casting method.[27] Therefore, the work function of various samples can be determined at a nanometer scale without any ambiguity. Real work function values were calculated from recorded CPD maps after calibration against a material of known work function (highly oriented pyrolytic graphite, HOPG). For the reference KPFM measurement, the HOPG surface was scanned employing the same experimental parameters and the VCPD (HOPG) was obtained. The work functions of measured samples were calculated by the following equation: φsample = VCPD (sample) -VCPD (HOPG) + φHOPG. Assuming a HOPG work function (φHOPG) = 4.6 eV.[33]

Characterization. The XPS measurements were performed using a Thermo Scientific ESCALAB 250Xi instrument equipped with Al Kα excitation source; Metal content of the samples were determined by inductively coupled plasma optical emission spectrometer (ICP-OES, PerkinElmer 7300DV); HR-TEM analysis for ND-based catalysts was conducted on Titan Themis ETEM G3 microscope with image corrector at 300 kV and Hitachi HF5000 with aberration-corrector at 200 kV. The EELS analyses were performed on STEM model on Hitachi HF5000 microscope with probe corrector at 200 kV cold-field emission gun. The energy resolution for the EELS system is better than 60 meV, which is determined from full-width at half-maximum (FWHM) of the zero-loss peak. Electron Paramagnetic Resonance (EPR) measurements were performed with an EPR X-band spectrometer (Bruker A200) at RT with samples sealed in a quartz sample tube. UV–vis absorption spectrum was obtained by UV–vis spectrometer (SHIMADZU UV2600). ATR-IR was performed under vacuum by the Vertex 70v spectrometer (Bruker) and samples were prepared by heating the mixture of I (1 mmol), model catalyst (0.1 mmol) and 10 ml toluene under 140 °C in O_2 with different reaction time (1, 2, 3, 4 and 5 h). The tests were carried out using a Veeco MultiMode 3D atomic force microscope (AFM) with a conductive noncontact cantilever coated with Pt/Ir and a nominal resonance frequency of 71.6 kHz.

Computational Details. All DFT calculations were performed by using Vienna ab initio Simulation Package (VASP).[37, 38] The projector augmented wave (PAW) potentials were explored to describe ion-

electron interaction.[39] The electronic exchange and correlation effects were described by the generalized gradient approximation (GGA)[40] with the PerdewBurke-Ernzerhof (PBE)[41] functional. The kinetic energy cutoff of 400 eV was used. All the structures were fully relaxed, the convergence criteria for force and energy were set to be 10^{-5} eV and 10^{-2} eV/Å, respectively. The Brillouin zones were sampled at 1x1x1 by Monkhorst-Pack meshes due to the large systems[42]. The vacuum space of 25 Å was set to avoid the interaction between adjacent images. The semi-empirical dispersion-corrected DFT-D3 scheme proposed by Grimme was used to describe the van der Waals interaction[43]. A (3x3) supercell of diamond with the bottom carbon atoms saturated with hydrogen was built. The most stable crystalline plane (111) for diamond was used in this work.[37] Graphene cluster edged with hydrogen and doped pyridine-N were adopted and coated on diamond to simplify the hybrid models for calculation. For the O_2 molecule adsorbed on diamond coated with one N-doped graphene layer (NG@ND), diamond coated with two graphene layers and one N-doped graphene layer (NG-2G@ND) systems and four graphene layers coated with one N-doped graphene layer (NG-4G), the adsorption energies (E_{ads}) of O_2 adsorbed on adsorbates are calculated by the following equation (1):

$$E_{ads} = E_{O2@adsorbate} - E_{adsorbate} - E_{O2} \quad (1)$$

Where, $E_{O2@adsorbate}$, $E_{adsorbate}$, and E_{O2} refers to the total energies of O_2 adsorbed on adsorbate, isolated adsorbate, and the isolated O_2, respectively.

Declarations

Acknowledgements

This work was financially supported from the NSFC of China (Nos. 21872144 and 21972140), CAS Youth Innovation Promotion Association (2018220), LiaoNing Revitalization Talents Program (XLYC1907053), China Postdoctoral Science Foundation (2018M641726) and Talents Innovation Project of Dalian city (2017RQ032). The authors acknowledge Mr. Hiroaki Matsumoto from Hitachi High-Tech for his great help in HR-TEM and EELS data acquisition at HF5000 microscope. We sincerely cherish our memory to Prof. Dangsheng Su for his indispensable supports and fruitful discussions.

Author contributions

Y. Liu. and Q. G. designed the study, conducted the experiments, data analysis and co-wrote the manuscript. Q.G. performed the catalysts synthesis, catalytic performance test and structural characterizations. Y.Z. performed the DFT calculations. R.H., Y. Lin, C.X., Q.J., S.P., and G.C. participated in the analysis of characterizations and revise the manuscript. Y. Liu and G.C. supervised the project. All authors discussed the results and commented on the manuscript.

Competing Interests

The authors report no declarations of interest.

References

1. Chen Y. X., Qian L. F., Zhang W., Han B. Efficient Aerobic Oxidative Synthesis of 2-Substituted Benzoxazoles, Benzothiazoles, and Benzimidazoles Catalyzed by 4-Methoxy-TEMPO. *Angew. Chem. Int. Ed.* **47**, 9330-9333 (2008).
2. Blacker A. J., Farah M. M., Hall M. I., Marsden S. P., Saidi O., Williams J. M. Synthesis of benzazoles by hydrogen-transfer catalysis. *Org. Lett.* **11**, 2039-2042 (2009).
3. Chang J., Zhao K., Pan S. Synthesis of 2-arylbenzoxazoles via DDQ promoted oxidative cyclization of phenolic Schiff bases-a solution-phase strategy for library synthesis. *Tetrahedron Lett.* **43**, 951-954 (2002).
4. Park K. H., Jun K., Shin S. R., Oh S. W. 2-Arylbenzoxazoles from phenolic schiff's bases by thianthrene cation radical. *Tetrahedron Lett.* **37**, 8869-8870 (1996).
5. Beaulieu P. L., Haché B., von Moos E. A practical Oxone®-mediated, high-throughput, solution-phase synthesis of benzimidazoles from 1, 2-phenylenediamines and aldehydes and its application to preparative scale synthesis. *Synthesis* **2003**, 1683-1692 (2003).
6. Yu J., Xu J., Lu M. Copper-catalyzed highly efficient aerobic oxidative synthesis of benzimidazoles, benzoxazoles and benzothiazoles from aromatic alcohols under solvent-free conditions in open air at room temperature. *Appl. Organomet. Chem.* **27**, 606-610 (2013).
7. Reddy M. M., Nizam A., Pasha M. Zn $(OAc)_2$ center dot $2H_2O$-Catalyzed, Simple, and Clean Procedure for the Synthesis of 2-Substituted Benzoxazoles Using a Grindstone Method. *Synth. Commun.* **41**, 1838-1842 (2011).
8. Tang L., Guo X., Yang Y., Zha Z., Wang Z. Gold nanoparticles supported on titanium dioxide: an efficient catalyst for highly selective synthesis of benzoxazoles and benzimidazoles. *Chem. Commun.* **50**, 6145-6148 (2014).
9. Yoo W. J., Yuan H., Miyamura H., Kobayashi S. Facile Preparation of 2-Substituted Benzoxazoles and Benzothiazoles via Aerobic Oxidation of Phenolic and Thiophenolic Imines Catalyzed by Polymer-Incarcerated Platinum Nanoclusters. *Adv. Synth. Catal.* **353**, 3085-3089 (2011).
10. Yu C*., et al.* AgPd nanoparticles deposited on $WO_{2.72}$ nanorods as an efficient catalyst for one-pot conversion of nitrophenol/nitroacetophenone into benzoxazole/quinazoline. *J. Am. Chem. Soc.* **139**, 5712-5715 (2017).
11. Su D. S., Wen G., Wu S., Peng F., Schlögl R. Carbocatalysis in liquid-phase reactions. *Angew. Chem. Int. Ed.* **56**, 936-964 (2017).
12. Duan X., Sun H., Wang S. Metal-free carbocatalysis in advanced oxidation reactions. *Acc. Chem. Res.* **51**, 678-687 (2018).
13. Navalon S., Dhakshinamoorthy A., Alvaro M., Garcia H. Carbocatalysis by graphene-based materials. *Chem. Rev.* **114**, 6179-6212 (2014).
14. Hu F*., et al.* Graphene-catalyzed direct Friedel-Crafts alkylation reactions: mechanism, selectivity, and synthetic utility. *J. Am. Chem. Soc.* **137**, 14473-14480 (2015).

15. Yang H., Cui X., Dai X., Deng Y., Shi F. Carbon-catalysed reductive hydrogen atom transfer reactions. *Nat. Commun.* **6**, 1-11 (2015).
16. Zhang J., Liu X., Blume R., Zhang A., Schlögl R., Su D. S. Surface-modified carbon nanotubes catalyze oxidative dehydrogenation of n-butane. *Science* **322**, 73-77 (2008).
17. Lin Y., Wu K. H., Yu L., Heumann S., Su D. S. Efficient and Highly Selective Solvent-Free Oxidation of Primary Alcohols to Aldehydes Using Bucky Nanodiamond. *ChemSusChem* **10**, 3497-3505 (2017).
18. Lin Y., Li B., Feng Z., Kim Y. A., Endo M., Su D. S. Efficient metal-free catalytic reaction pathway for selective oxidation of substituted phenols. *ACS Catal.* **5**, 5921-5926 (2015).
19. Lin Y., Su D. Fabrication of nitrogen-modified annealed nanodiamond with improved catalytic activity. *ACS Nano* **8**, 7823-7833 (2014).
20. Duan X.*, et al.* Surface controlled generation of reactive radicals from persulfate by carbocatalysis on nanodiamonds. *Appl. Catal.s B Environ.* **194**, 7-15 (2016).
21. Duan X.*, et al.* Nanodiamonds in sp^2/sp^3 configuration for radical to nonradical oxidation: Core-shell layer dependence. *Appl. Catal. B Environ.* **222**, 176-181 (2018).
22. Guo D., Shibuya R., Akiba C., Saji S., Kondo T., Nakamura J. Active sites of nitrogen-doped carbon materials for oxygen reduction reaction clarified using model catalysts. *Science* **351**, 361-365 (2016).
23. Lin Y.*, et al.* Highly Efficient Metal-Free Nitrogen-Doped Nanocarbons with Unexpected Active Sites for Aerobic Catalytic Reactions. *ACS Nano* **13**, 13995-14004 (2019).
24. Lin Y., Sun X., Su D. S., Centi G., Perathoner S. Catalysis by hybrid sp^2/sp^3 nanodiamonds and their role in the design of advanced nanocarbon materials. *Chem. Soc. Rev.* **47**, 8438-8473 (2018).
25. Qin R., Liu K., Wu Q., Zheng N. Surface coordination chemistry of atomically dispersed metal catalysts. *Chem. Rev.* **120**, 11810-11899 (2020).
26. Liu D.*, et al.* Atomically dispersed platinum supported on curved carbon supports for efficient electrocatalytic hydrogen evolution. *Nat. Energ.* **4**, 512-518 (2019).
27. Jia Y.*, et al.* Identification of active sites for acidic oxygen reduction on carbon catalysts with and without nitrogen doping. *Nat. Catal.* **2**, 688-695 (2019).
28. Lin Y.*, et al.* Overall Oxygen Electrocatalysis on Nitrogen-Modified Carbon Catalysts: Identification of Active Sites and In Situ Observation of Reactive Intermediates. *Angew. Chem. Int. Ed.* **60**, 3299-3306 (2020).
29. Gong K., Du F., Xia Z., Durstock M., Dai L. Nitrogen-doped carbon nanotube arrays with high electrocatalytic activity for oxygen reduction. *Science* **323**, 760-764 (2009).
30. Osswald S., Mochalin V., Havel M., Yushin G., Gogotsi Y. Phonon confinement effects in the Raman spectrum of nanodiamond. *Phys. Rev. B* **80**, 075419 (2009).
31. Crane M. J.*, et al.* High-pressure, high-temperature molecular doping of nanodiamond. *Sci. Adv.* **5**, 6073-6080 (2019).
32. Cheon J. Y., Kim J. H., Kim J. H., Goddeti K. C., Park J. Y., Joo S. H. Intrinsic relationship between enhanced oxygen reduction reaction activity and nanoscale work function of doped carbons. *J. Am.*

Chem. Soc. **136**, 8875-8878 (2014).

33. Wrana D., Cieślik K., Belza W., Rodenbücher C., Szot K., Krok F. Kelvin probe force microscopy work function characterization of transition metal oxide crystals under ongoing reduction and oxidation. *Beilstein J. Nanotech.* **10**, 1596-1607 (2019).
34. Zhang C., Li T., Zhang J., Yan S., Qin C. Degradation of p-nitrophenol using a ferrous-tripolyphosphate complex in the presence of oxygen: The key role of superoxide radicals. *Appl. Catal. B Environ.***259**, 118030 (2019).
35. Yamakoshi Y., Sueyoshi S., Fukuhara K., Miyata N., Masumizu T., Kohno M. •OH and $O_2^{\bullet-}$Generation in Aqueous C_{60} and C_{70} Solutions by Photoirradiation: An EPR Study. *J. Am. Chem. Soc.* **120**, 12363-12364 (1998).
36. Su C.*, et al.* Probing the catalytic activity of porous graphene oxide and the origin of this behaviour. *Nat. Commun.* **3**, 1-9 (2012).
37. Jaimes R., Vazquez-Arenas J., González I., Galván M. J. S. S. Delimiting the boron influence on the adsorptive properties of water and OH radicals on H-terminated Boron Doped Diamond catalysts: A Density Functional Theory analysis. *Surf. Sci.* **653**, 27-33 (2016).
38. Kundu S.*, et al.* Electrocatalytic activity and stability of nitrogen-containing carbon nanotubes in the oxygen reduction reaction. *J. Phys. Chem. C* **113**, 14302-14310 (2009).
39. Duan X.*, et al.* Nitrogen-doped graphene for generation and evolution of reactive radicals by metal-free catalysis. *ACS Appl. Mater. Inter.* **7**, 4169-4178 (2015).
40. Perdew J. P., Burke K., Ernzerhof M. Generalized gradient approximation made simple. *Phys. Rev. Lett.* **77**, 3865 (1996).
41. Perdew J. P., Ernzerhof M., Burke K. Rationale for mixing exact exchange with density functional approximations. *J. Chem. phys.* **105**, 9982-9985 (1996).
42. Monkhorst H. J., Pack J. D. Special points for Brillouin-zone integrations. *Phys. Rev. B* **13**, 5188 (1976).
43. Grimme S. Semiempirical GGA-type density functional constructed with a long-range dispersion correction. *J. Comp. Chem.* **27**, 1787-1799 (2006).

Table

Due to technical limitations Table 1 is available as a download in the Supplementary Files.

Figures

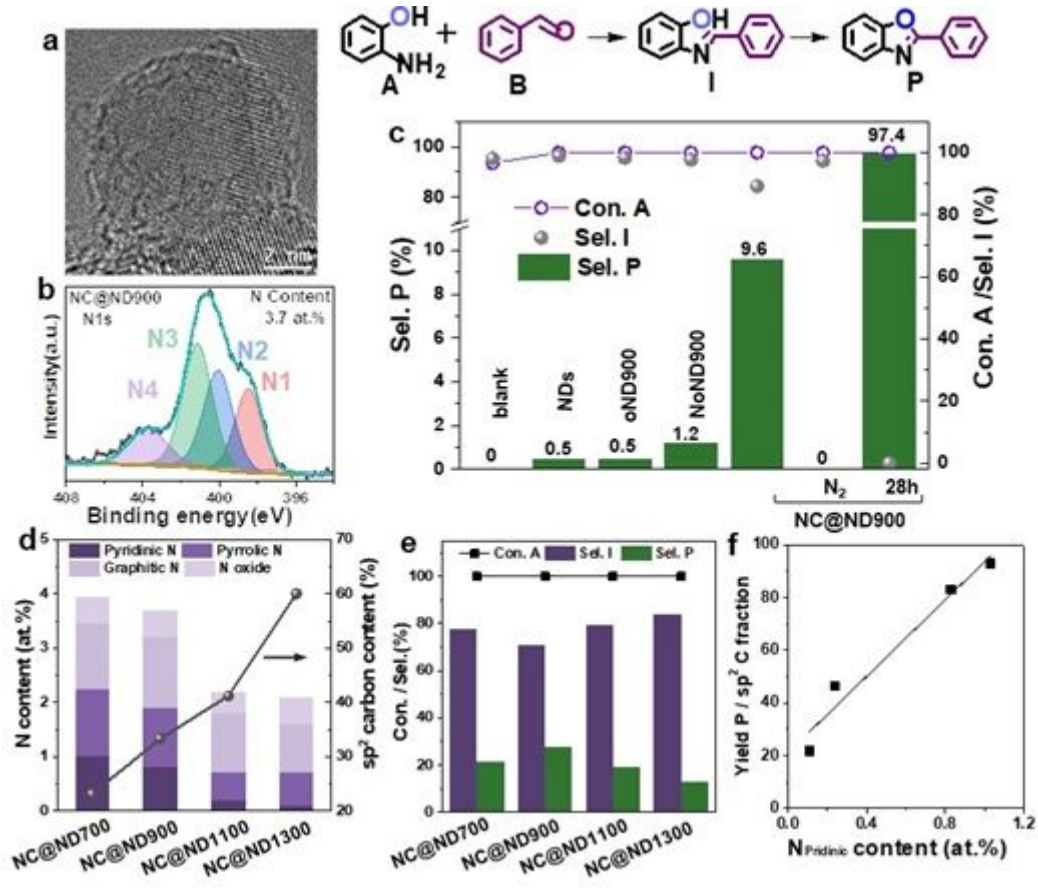

Figure 1

The catalytic performance of N-doped sp3@ sp2 hybrid nanocarbons. (a) HR-TEM image and (b) XPS N1s spectrum of NC@ND-900; (c) Catalytic performance of different NDs-based catalysts. Reaction conditions: 2 mmol aminophenol, 2.2 mmol benzaldehyde, 10 mL xylene, 40 mg catalyst , 140 °C, t = 2 h, 1 atm O2; Quantitative analysis was carried out by GC using nitrobenzene as internal standard; (d) N content, N species distribution and sp2 carbon content derived from XPS of various N-doped sp3@sp2 nanocarbon annealed under different temperature; (e) Catalytic performance of various N-doped sp3@sp2 nanocarbon annealed under different temperature. Reaction conditions: 2 mmol aminophenol, 2.2 mmol benzaldehyde, 10 mL xylene, catalyst 120 mg, 140 °C, t = 2 h, 1 atm O2; (f) Relationships between pyridinic N content and yield of 2-phenylbenzoxazole normalized by sp2 carbon fraction.

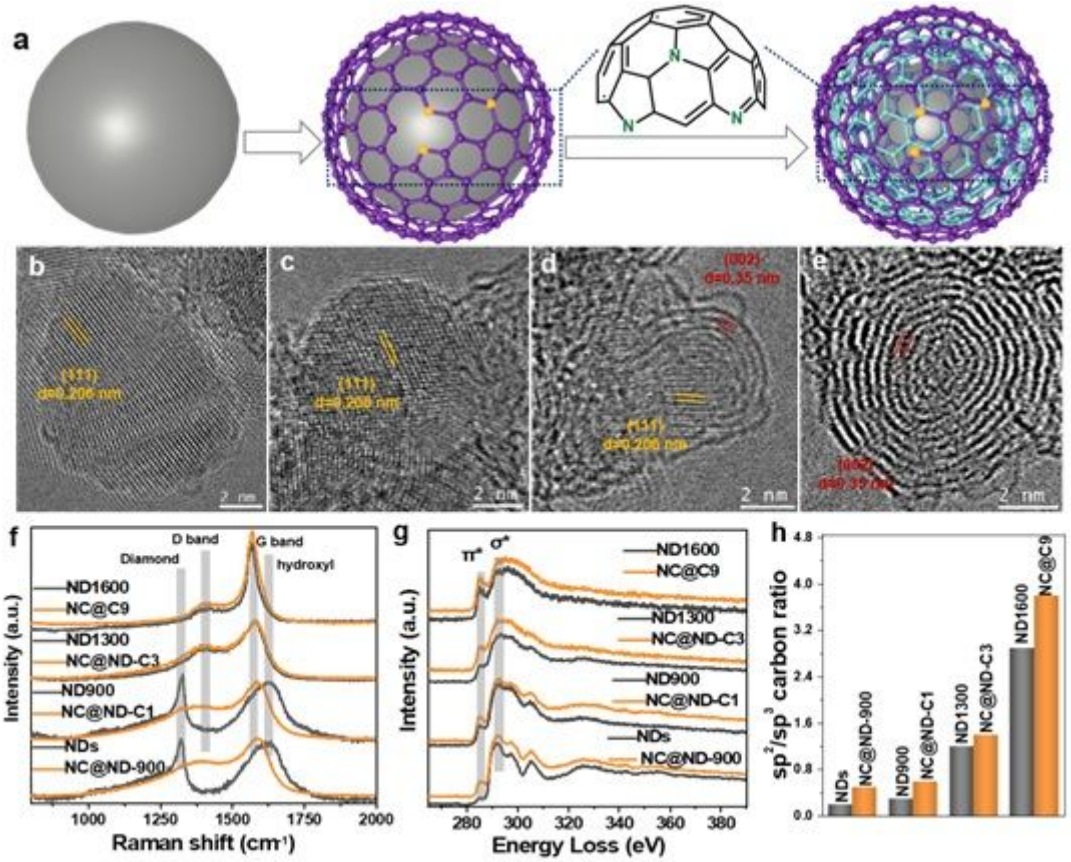

Figure 2

The influence of sp2 C layers on the catalytic activity of pyridinic N sites. (a) Schematic illustration of catalyst design process: catalytically active N groups introduction and the regulation of sp2 carbon layers. HR-TEM images of (b) pristine NDs, (c) NC@ND- C1, (d) NC@ND-C3 and (e) NC@C9.The scale bar is 2 nm; (f) UV-Raman spectra (λ=325 nm) of NDs and N-doped sp3@sp2 nanocarbon; (g) EELS profiles of NDs and N-doped sp3@sp2 nanocarbon; (h) sp2/sp3 carbon ratios derived from XPS C1s spectra results.

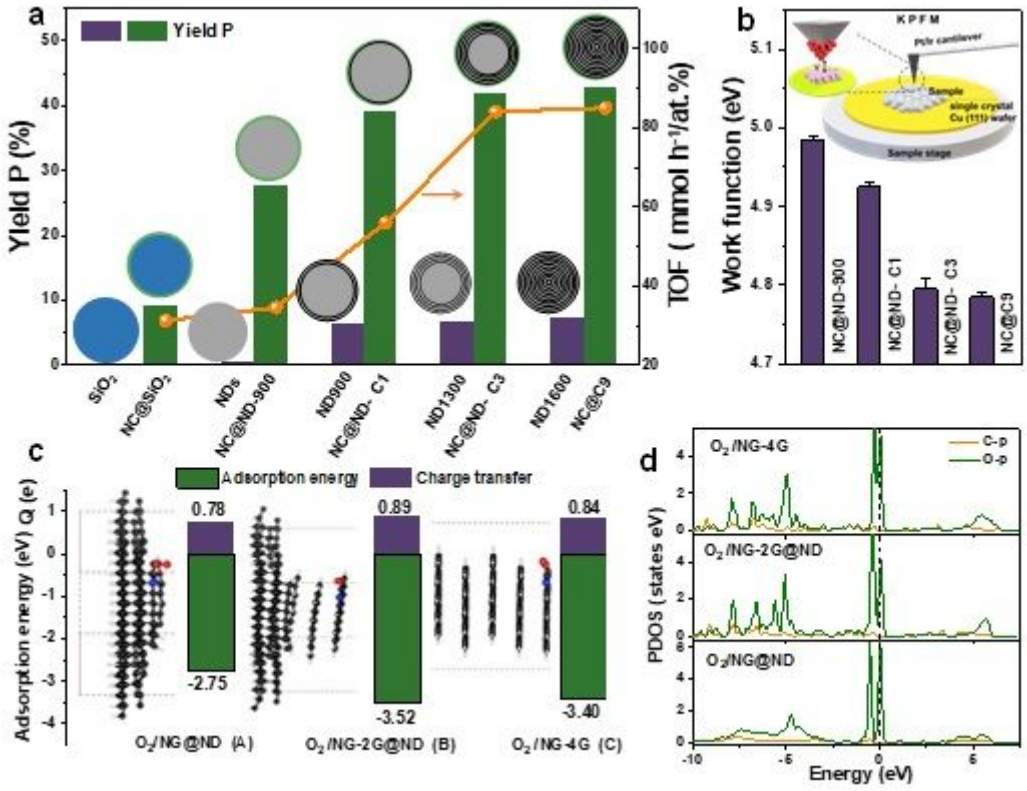

Figure 3

Probing the origin of enhanced catalytic performance of pyridinic N sites by regulating sp2 C layers. (a) Catalytic performance and pyridinic N content normalized reaction rate of P (λP) of various N-free and N-doped sp3@sp2 nanocarbon. Reaction conditions: 2 mmol aminophenol, 2.2 mmol benzaldehyde, 10 mL xylene, 120 mg catalyst, 140 °C, t = 2 h, 1 atm O2. Quantitative analysis was determined by GC-FID using nitrobenzene as internal standard; (b) The local work functions collected from the NC@ND-900, NC@ND-C1, NC@ND- C3 and NC-C9 by KPFM measurements. The inset shows the scheme of the KPFM test. (c) Adsorption energy of O2 on structure A, structure B and structure C and Charge tranfer (Q) to the adsorbed O2 obtained by Bader charge analysis. The inset shows the side views of optimized configurations. (d) Calculated PDOS for the p orbital of the C atoms that bind with the O2 and p orbital of the adsorbed O2 for O2/NG@ND, O2/NG-2G@ND and O2/NG-4G. The Fermi level is set at the zero of energy (dashed line in figures).

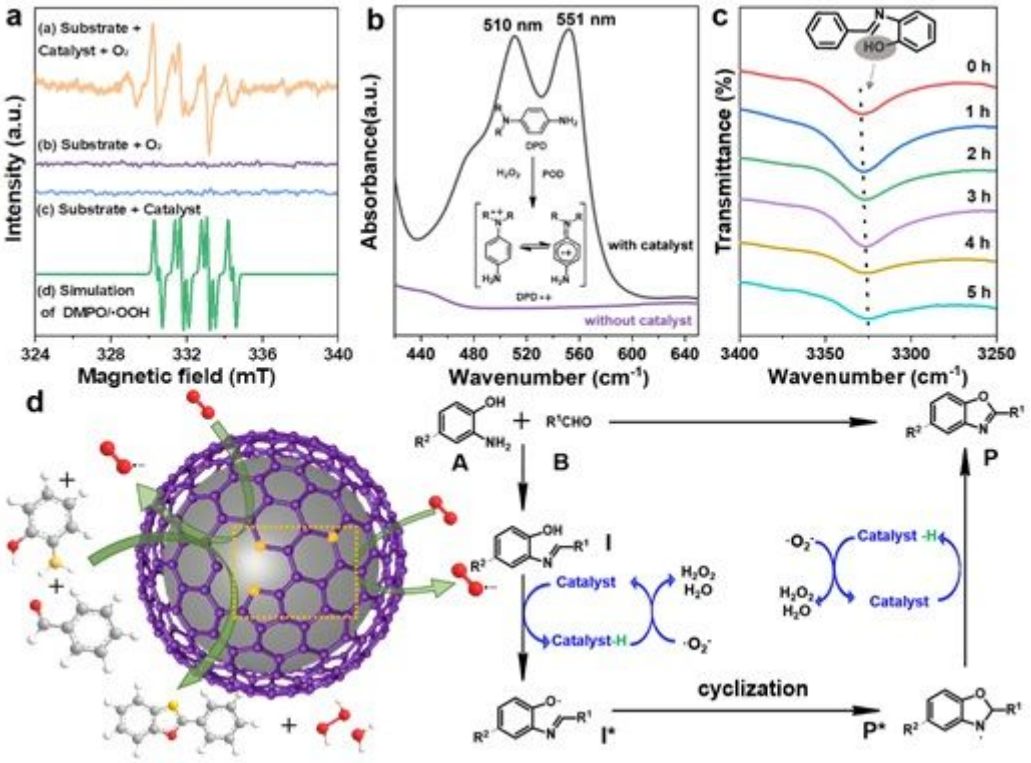

Figure 4

Mechanistic Study of N-doped sp3@ sp2 nanocarbons catalyzed aerobic synthesis of 2-phenylbenzoxazole process. (a) The EPR spectra of different reaction systems with DMPO as radical trap; (b) The ultraviolet-visible absorption spectra of the reaction system (with and without catalyst) after adding DPD and POD; (c) ATR-IR spectrum of catalytic systems with I as reactant, 1,10-phenanthroline as model catalyst and toluene as solvent under 140 °C in O2 for 1, 2, 3, 4 and 5 h, respectively; (d) Schematic representation of the proposed mechanism of N-doped sp3@sp2 nanocarbon catalyzed aerobic synthesis of 2-substituted benzoxazoles.

Supplementary Files

This is a list of supplementary files associated with this preprint. Click to download.

- supportinginformation.docx
- Scheme1.pdf
- Table1.pdf